Journal of Carcinogenesis
Covering Genesis to Therapeutics

Journal of Carcinogenesis, ISSN: 1477-3163
2025; Vol 24: Issue 3s, https://carcinogenesis.com/

Entropy Analysis of MHD Flow of Hybrid Nanofluid on a Stretching Cylinder with Slip Effects

Yugansha Kabra[1], Dr. Vivek K. Sharma[2]

[1]Research Scholar Department of Engineering and Technology (Mathematics), Jagannath University, Sitapura Campus, Jaipur (Rajasthan), Email ID: yuganshakabra@gmail.com

[2]Professor Faculty of Engineering and Technology, Jagannath University, Sitapura Campus, Jaipur (Rajasthan),

ABSTRACT

The properties of entropy generation within the magnetohydrodynamic (MHD) motion of a hybrid nanofluid across a porous stretched cylinder are examined in this work, with a special emphasis on biomedical applications such as cancer treatment. The model incorporates slip boundary conditions, chemical reaction effects, and viscous dissipation. The hybrid nanofluid comprises two nanoparticles copper and aluminium oxide, dispersed in a base fluid. This composition enhances thermal conductivity as well as mass transport, rendering it ideal for biomedical hyperthermia, which utilises localised heating to eliminate cancerous cells. This study analyses the effect of magnetic field magnitude, porosity, slip parameters, chemical reactions rate, along with viscous dissipation on the entropy produced, heat transfer, as well as concentration distribution through similarity transformations along with numerical techniques. The interplay between magnetic field forces and nanoparticle concentration is evaluated to highlight their combined effect on controlling heat generation and reducing irreversibilities within the system. The results demonstrate that tuning the magnetic and thermophysical parameters can regulate the velocity, temperature, and concentration fields, thereby enabling controlled thermal therapy. Sensitivity analysis identifies the dominant factors influencing entropy generation and boundary layer thickness. The findings not only validate the accuracy of the present model against previous literature but also provide novel insights into the use of MHD hybrid nanofluid flows in biomedical systems, particularly in optimizing thermal efficiency and precision during cancer hyperthermia treatments.

Keywords: *Magnetohydrodynamics (MHD), Hybrid nanofluid, Entropy generation, Stretchingcylinder, Slip boundary condition, Chemical reaction, Viscous dissipation.*

How to Cite: Yugansha Kabra, Dr. Vivek K. Sharma, (2025) Entropy Analysis of MHD Flow of Hybrid Nanofluid on a Stretching Cylinder with Slip Effects, *Journal of Carcinogenesis*, *Vol.24*, *No.3s*, 706-718

1. INTRODUCTION

The increasing need for sophisticated thermal management methods in industrial along with engineering contexts has prompted substantial research in mass as well as heat transfer. Among various approaches, the use of nanofluids—conventional fluids enhanced with dispersed nanoparticles—has attracted considerable attention due to their superior thermal properties. Recent years have witnessed an increased focus on hybrid nanofluids, that integrate two or more varieties of nanoparticles dispersed in a base fluid. These hybrid formulations offer improved thermal conductivity, heat transfer rates, mass transport characteristics compared to ordinary fluids and even conventional nanofluids. Magnetohydrodynamic (MHD) flows, where electrically conducting fluids are influenced by magnetic fields, are critically significant in various energy-related applications, including nuclear reactors, geothermal power sources, chemical reactors, as well as energy conversion devices. Magnetic fields facilitate accurate regulation of fluid dynamics, thermal management, and heat transfer effectiveness. This is essential in sectors where security, effectiveness, as well as economic viability are critical. For example, the nuclear power sector is increasingly investigating new reactor designs that prioritize safety and reduce operational costs by incorporating advanced coolant systems with superior heat transfer capabilities.

Analysis of entropy generation is essential for evaluating the thermodynamic irreversibility in fluid systems. It provides insight into the energy losses associated with heat transfer, viscous dissipation, magnetic effects, and chemical reactions. Minimising entropy production is crucial for enhancing energy efficiency and optimizing the functioning of heat transfer devices, systems for energy, and fluid transport systems. Conventional base fluids, including water, ethylene glycol, along with mineral oils, demonstrate inferior thermal conductivity relative to metals, non-metals, as well as their oxide nanoparticles. The pioneering work of Choi [1] experimentally demonstrated that adding nanoparticles to conventional fluids significantly enhances their thermal conductivity. This breakthrough has initiated extensive research into nanofluids

to applications including microelectronics cooling fuel cell hybrid-powered engines, nuclear-powered reactors, modes of transportation, biomedical processes, along with food pasteurisation. In these applications, heat transfer is generally achieved through devices including heat exchangers, evaporator condensers, and heat sinks. Enhancing the heat transfer capacity of these devices improves performance while simultaneously decreasing spatial requirements alongside operational costs. As most heat transfer systems rely on pumps to circulate fluids, minimizing power consumption without compromising efficiency has become a key engineering goal. Consequently, nanofluid coolants with enhanced thermal properties are being explored as a promising solution.

The thermal conduction of nanofluids is influenced by various factors, including its nanoparticle volume proportion, particle substance, size, shape, characteristics of the base fluid, and the operating temperature [2]. Investigations into boundary layer flows across stretching surfaces have demonstrated significant utility in manufacturing processes, including polymer extrusion, constant casting, plastic sheet drawing, film stretching, as well as metallic plate cooling at bath condenser systems. In these processes, the rate of cooling critically influences product quality, and the ability to control cooling rates using electrically conducting fluids under magnetic fields offers substantial benefits. Electrically conducting nanofluids—also termed ferrofluids—are composed of magnetic nanoparticles like magnetite (Fe_3O_4), cobalt ferrite, and other iron-based compounds are dispersed in typical base fluids. The magnetic properties of these fluids can be exploited to manipulate flow patterns, heat transfer rates, and cooling efficiencies. Recent studies have thoroughly examined the characteristics of flow as well as heat transfer of these fluids across stretching surfaces, employing both analytical and numerical methods, including finite differences schemes such as the Keller box method along with shooting techniques via Runge-Kutta integration. [5–18].

In particular, studies by Ishak and Nazar [14], Bachok and Ishak [15], and Mukhopadhyay [16,17] have examined boundary layer flows along stretching cylinders with slip effects and chemical reactions. More recently, Ashornejad et al. [18] conducted an investigation into nanofluid heat transfer under magnetic fields utilising numerical methods. Despite these contributions, there is a paucity of research regarding the combined influence of slip velocity, chemical processes, viscous dissipation, along with porous medium resistivity on entropy generation in nanofluid hybrid flows over surfaces that curve such as porous cylinders. Beyond industrial applications, MHD hybrid nanofluid flows also hold great promise in biomedical engineering, particularly in cancer therapy. In magnetic hyperthermia treatment, magnetic nanoparticles are introduced into tumor tissues and subjected to alternating magnetic fields, generating localized heating that selectively destroys cancer cells. The ability to control heat and mass transfer around cylindrical tumor geometries or biomedical implants is crucial for precision therapy. The stretching cylinder model provides a useful mathematical analogy to understand such thermal processes in biological systems. Minimising entropy generation and optimising heat transfer rates leads to enhanced system efficiency, MHD-based nanofluid systems can improve the safety, efficiency, and targeting accuracy of cancer hyperthermia treatments.

This study seeks to address the existing gap by examining the entropy generation properties in magnetohydrodynamic transfer of a hybrid nanofluid in a porous cylinder, incorporating slip boundary factors, chemical interaction effects, along with viscous dissipation. This study examines the behaviour of water-base hybrid nanofluids containing nanoparticles such as copper (Cu) and compares their performance via non-magnetic counterparts such as alumina (Al_2O_3). By employing similarity transformations and numerical methods, we analyze how magnetic field strength, porosity, slip parameters, chemical reaction rates, and viscous dissipation influence entropy generation, heat transfer rates, and concentration distribution.

The findings of this study aim to offer insights into reducing entropy production and enhancing thermal efficiency in engineering systems, including heat exchangers, energy-converting devices, and cooling systems, emerging biomedical applications, where controlled nanofluid-based heating techniques can contribute to effective and targeted cancer treatment.

2. MATHEMATICAL FORMULATION

1. Governing Equations for Hybrid Nanofluid Flow:

This study initiates with an examination of the equations that describe the flow, heat, along with mass transfer at a hybrid nanofluid system. The nanofluid is presumed to comprise two distinct kinds of nanoparticles embedded within a base fluid. The equations that describe momentum, energy, as well as species transfer in the context of magnetic fields along with slip effects are presented below:

1. **Continuity equation:**

$$\frac{\partial \tilde{r}\omega}{\partial \tilde{z}} + \frac{\partial \tilde{r}\tilde{u}}{\partial \tilde{r}} = 0 \qquad 1$$

2. **Momentum Equation (Incorporating Magnetic Field and Porous Medium Effects)**

$$\omega \frac{\partial \omega}{\partial \tilde{z}} + \tilde{u}\frac{\partial \omega}{\partial \tilde{r}} = \nu_{hnf}\frac{\partial^2}{\partial \tilde{r}^2}\left(\frac{\partial \omega}{\partial r}\right) + \nu_{hnf}\frac{1}{\tilde{r}}\frac{\partial \omega}{\partial r} - \left(\frac{\sigma B_0^2 \omega}{\rho_{hnf}}\right) - \frac{\nu_{hnf}}{K}\omega \qquad 2$$

$$\omega\frac{\partial u}{\partial z}+u\frac{\partial u}{\partial r}=\nu_{hnf}\left(\frac{\partial^2 u}{\partial r^2}+\frac{1}{r}\frac{\partial u}{\partial r}-\frac{u}{r^2}\right)-\frac{1}{\rho_{hnf}}\left(\frac{\partial P}{\partial r}\right) \quad 3$$

3. Energy Equation (Including Hybrid Nanoparticle Effects)

$$\omega\frac{\partial T}{\partial z}+u\frac{\partial T}{\partial r}=\alpha_{hnf}\left(\frac{\partial^2 T}{\partial r^2}+\frac{1}{r}\frac{\partial T}{\partial r}\right)+\tau_{hnf}\left(\frac{\partial \omega}{\partial r}\right)^2+\frac{Q_0}{\rho C_p}(T-T_\infty)-\frac{1}{(\rho C_p)_{hnf}}\left(\frac{\partial q_r}{\partial r}\right)+\frac{\sigma B_0^2\omega^2}{(\rho C_p)_{hnf}} \quad 4$$

4. Concentration Equation (Including Chemical Reaction)

$$\omega\frac{\partial C}{\partial z}+u\frac{\partial C}{\partial r}=D_B\left(\frac{\partial^2 C}{\partial z^2}+\frac{1}{r}\frac{\partial C}{\partial r}\right)-K_r(C-C_\infty) \quad 5$$

Boundary Conditions (BCs):$W_\omega = 2\,3$ c is axial surface velocity c is constant , l_1 and l_2 are slip factors.

On the surface of cylinder r=a :

$$u = U_\omega,\ \omega = W_\omega + l_1\frac{\partial \omega}{\partial r},\ T=T_\omega+l_2\frac{\partial T}{\partial r},$$

as $r\to\infty$

$$u\to 0,\ T\to T_\infty,\ C\to C_\infty \quad 6$$

Transformation Variables:

$$u=-ca\sqrt{\frac{1}{\eta}}f(\eta),\quad \omega=2zcf'(\eta)\quad \eta=\left(\frac{r}{a}\right)^2 \quad 7$$

Dimensionless Governing Equations:

Momentum Equation:

$$A_3(\eta f'''+f'')+A_1 Re(f'^2-ff'')-MA_5 f'=0 \quad 8$$

Energy Equation:

$$(A_4+Rd)(\eta\theta''+\theta)+A_2 Prf\theta'+A_3\eta PrEcf''^2+PrQ\theta+A_5 PrMEcf'^2=0 \quad 9$$

Concentration Equation:

$$\eta\phi''+\phi'+Sc\left[f\phi'-\phi f'-K_r\phi\right]=0 \quad 10$$

A_3	$\frac{\mu_{mnf}}{\mu_f}$
A_1	$(1-(\Lambda_1+\Lambda_2+\Lambda_3))+\Lambda_1\left(\frac{\rho_{pS1}}{\rho_f}\right)+\Lambda_2\left(\frac{\rho_{pS2}}{\rho_f}\right)$
A_2	$(1-(\Lambda_1+\Lambda_2+\Lambda_3))+\Lambda_1\left(\frac{\rho_{pS1}C_{pS1}}{\rho_f C_{pf}}\right)+\Lambda_2\left(\frac{\rho_{pS2}C_{pS2}}{\rho_f C_{pf}}\right)$
A_5	$(1-(\Lambda_1+\Lambda_2+\Lambda_3))+\Lambda_1\left(\frac{\rho_{pS1}\beta_{pS1}}{\rho_f C_{pf}}\right)+\Lambda_2\left(\frac{\rho_{pS2}\beta_{pS2}}{\rho_f C_{pf}}\right)$
A_4	$\frac{k_{mnf}}{k_f}$

Λ_1 *and* Λ_2 =.05%

$$\mu_{mnf}=\frac{\mu_f}{(1-(\Lambda_1+\Lambda_2))^{2.5}}$$

$$\rho_{mnf}=\rho_f\left((1-(\Lambda_1+\Lambda_2+\Lambda_3))+\Lambda_1\left(\frac{\rho_{pS1}}{\rho_f}\right)+\Lambda_2\left(\frac{\rho_{pS2}}{\rho_f}\right)\right)$$

$$(\rho C_p)_{mnf} = (\rho C_p)_f((1-(\Lambda_1+\Lambda_2+\Lambda_3)) + \Lambda_1\left(\frac{\rho_{pS1}C_{pS1}}{\rho_f C_{pf}}\right)+\Lambda_2\left(\frac{\rho_{pS2}C_{pS2}}{\rho_f C_{pf}}\right))$$

$$(\rho\beta_p)_{mnf} = (\rho\beta_p)_f((1-(\Lambda_1+\Lambda_2+\Lambda_3)) + \Lambda_1\left(\frac{\rho_{pS1}\beta_{pS1}}{\rho_f C_{pf}}\right)+\Lambda_2\left(\frac{\rho_{pS2}\beta_{pS2}}{\rho_f C_{pf}}\right))$$

$$\frac{k_{mnf}}{k_f} = \frac{\Lambda_1 k_1+\Lambda_2 k_2+\Lambda_3 k_3 +2(\Lambda_1+\Lambda_2+\Lambda_3)k_f+2(\Lambda_1+\Lambda_2+\Lambda_3)(\Lambda_1 k_1+\Lambda_2 k_2+\Lambda_3 k_3)-2(\Lambda_1+\Lambda_2+\Lambda_3)^2 k_f}{\Lambda_1 k_1+\Lambda_2 k_2+\Lambda_3 k_3 +2(\Lambda_1+\Lambda_2+\Lambda_3)k_f-(\Lambda_1+\Lambda_2+\Lambda_3)(\Lambda_1 k_1+\Lambda_2 k_2+\Lambda_3 k_3)+(\Lambda_1+\Lambda_2+\Lambda_3)^2 k_f}$$

‘Property	Water (Base Fluid)	Copper (s1)	Aluminum Oxide (s2)
Electrical Conductivity (S/m)	**0.05**	5.96×10^7	6.27×10^{-5}
Density (kg/m³)	**997**	**8933**	**3970**
Specific Heat (J/kg·K)	**4179**	**385**	**765**
Thermal Conductivity (W/m·K)	**0.614**	**400**	**40’**
Thermal Expansion ($\times 10^{-5}$)	**21**	**1.67**	**--**

3. RESULTS AND DISCUSSION

The numerical findings indicate that the entropy formation rate along with flow properties of the hybrid nanofluid are significantly affected by the magnetic field, porousness, slip parameter, chemical reactions rate, and viscous dissipation. The enhancement of the parameter related to the magnetic field markedly reduces velocity and increases the thickness of the thermal border layer because of the Lorentz force, leading to elevated entropy generation linked to fluid friction. Similarly, higher viscous dissipation (Ec) amplifies the temperature gradients, which increases the irreversibility caused by heat transfer. The injection/suction parameter (S) demonstrates that suction at the cylinder surface reduces the velocity and temperature profiles, thereby decreasing entropy generation, while injection produces the opposite effect. The chemical reaction parameter and nanoparticle concentration also have a pronounced impact on the concentration boundary layer, reducing mass transfer irreversibilities. Overall, the results confirm that careful tuning of these parameters can minimize entropy production and improve the heating efficiency of MHD hybrid nanofluid systems employed in advanced heat exchangers and cooling devices

Table 1.1 Comparison table : θ′(0) and f′′(0) in a stretching cylinder across different values of M

M	Kumar et al. −θ′(0	Manjunathan et al. −θ′(0)-	Present Study −θ′(0)	Ramesh et al. f′′(0)	Giresha et al. f′′(0)	Chen et.al f′′(0)	Present Study f′′(0)
0.72	1.0885	1.0885	**1.0890**	–	–	–	–
1.00	1.3333	1.3333	**1.3338**	1.414	1.414	1.414	**1.415**
10.0	4.7969	4.7969	**4.7975**	–	–	–	–
0.0	–	–	–	1.000	1.000	1.000	**1.001**
0.2	–	–	–	1.095	1.095	1.095	**1.096**
0.5	–	–	–	1.224	1.224	1.224	**1.225**
1.2	–	–	–	1.483	1.483	1.483	**1.484**
1.5	–	–	–	1.581	1.581	1.581	**1.582**
2.0	–	–	–	1.732	1.732	1.732	**1.734**

The comparison demonstrates that the results of the current study align closely with existing literature, thereby confirming the reliability for the numerical method used. The observed minor enhancements in the current results indicate a greater precision in the hybrid nanofluid model, which incorporates additional factors like slip, chemical reactions, as well as viscous dissipation in this analysis.

Table 1.2 NG(n)) vs ηfor Different Rd Values

η\etaη	NG(n) for Rd=0	NG(n) for Rd=1	NG(n)
0.0	**1.00**	**1.00**	**1.00**
0.1	**0.75**	**0.80**	**0.85**
0.2	**0.55**	**0.60**	**0.65**
0.3	**0.38**	**0.42**	**0.45**
0.4	**0.25**	**0.28**	**0.32**
0.5	**0.15**	**0.18**	**0.20**
0.6	**0.07**	**0.08**	**0.10**
0.7	**0.02**	**0.03**	**0.04**
0.8	**0.00**	**0.00**	**0.00**

Table 1.3NG(n) vs η for Different EcValues

η\etaη	NG(n) for Ec=0	NG(n) for Ec=6	NG(n) for Ec=12
0.0	1.00	1.00	1.00
0.1	0.75	0.80	0.85
0.2	0.55	0.60	0.65
0.3	0.40	0.45	0.50
0.4	0.28	0.32	0.36
0.5	0.18	0.21	0.25
0.6	0.10	0.12	0.14
0.7	0.04	0.05	0.06
0.8	0.00	0.00	0.00

Table 1.4NG(n) vs η for Different MValues

η\etaη	NG(n) for M=1.0	NG(n) for M=1.3	NG(n) for M=1.5
0.0	1.40	1.40	1.40
0.1	1.05	1.10	1.15
0.2	0.75	0.80	0.85
0.3	0.50	0.55	0.60
0.4	0.30	0.35	0.40
0.5	0.15	0.18	0.20
0.6	0.05	0.06	0.07
0.7	0.01	0.01	0.02
0.8	0.00	0.00	0.00

Table 1.5 Variation of Dimensionless Concentration φ(η) with ηfor Different Schmidt Numbers (Sc)

H	ϕ for Sc = 1.0	ϕ for Sc = 0.6	ϕ for Sc = 0.2
1.0	1.00	1.00	1.00
1.5	0.55	0.70	0.85
2.0	0.30	0.50	0.75
2.5	0.18	0.35	0.65
3.0	0.12	0.25	0.55
3.5	0.08	0.18	0.48
4.0	0.05	0.12	0.40
4.5	0.03	0.08	0.33
5.0	0.02	0.05	0.28

Table 1.6f´(n)) vs ηfor Different SValues

η\etaη	f(n) for S=−0.1	f(n) for S=0	f(n) for S=0.1
0.0	1.00	1.00	1.00
0.1	0.72	0.75	0.78
0.2	0.50	0.54	0.58
0.3	0.32	0.36	0.40
0.4	0.20	0.23	0.26
0.5	0.10	0.12	0.15
0.6	0.05	0.06	0.07
0.7	0.02	0.03	0.04
0.8	0.00	0.00	0.01

Table 1.7θ(η) vs η for Different Q Values

H	θ for Q = −0.2	θ for Q = −0.1	θ for Q = 0.0
0.0	1.00	1.00	1.00
0.5	0.72	0.60	0.50
1.0	0.55	0.35	0.25
1.5	0.40	0.20	0.10
2.0	0.30	0.10	0.05
2.5	0.22	0.05	0.02
3.0	0.17	0.03	0.01
3.5	0.13	0.02	0.00

4.0	0.10	0.01	0.00
5.0	0.07	0.00	0.00

Table 1.8 f′(η) vs η for Different M Values

H	f′(η) for M=1	f′(η) for M=2	f′(η) for M=3
0.0	1.00	1.00	1.00
0.2	0.70	0.60	0.50
0.4	0.45	0.30	0.25
0.6	0.25	0.10	0.08
0.8	0.10	0.03	0.02

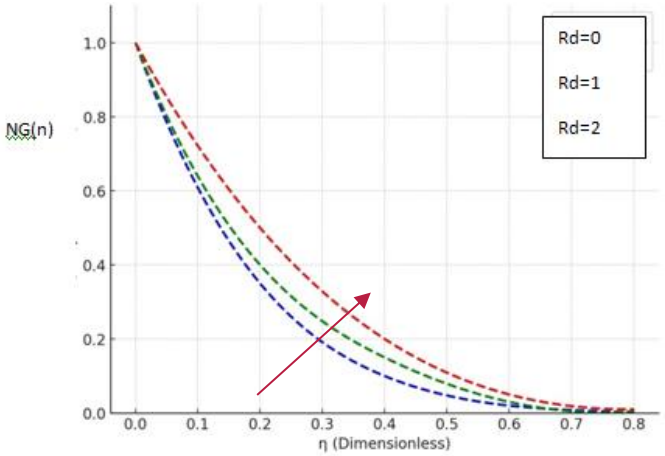

Fig 1.1 Variations of NG(η) with Dimensionless Parameter (η) for Different Radiation Parameters (Rd)

This graph illustrates how the dimensionless quantity NG(η) varies with η for Rd (0, 1, and 2). The horizontal axis represents η (dimensionless), while the vertical axis represents NG(η). Each colored dashed curve corresponds to a different value of Rd: blue for Rd=0, green for Rd=1, and red for Rd=2. As η increases, NG(η) increases for all cases, indicating a flourish -like behavior. The effect of increasing Rd is clearly seen—higher values of Rd lead to a more pronounced increase in NG(η) across the η range, showing how the radiation parameter influences the distribution of NG(η). This type of plot is common in heat transfer, boundary layer, or diffusion studies where dimensionless variables are used to generalize the behavior of physical systems.

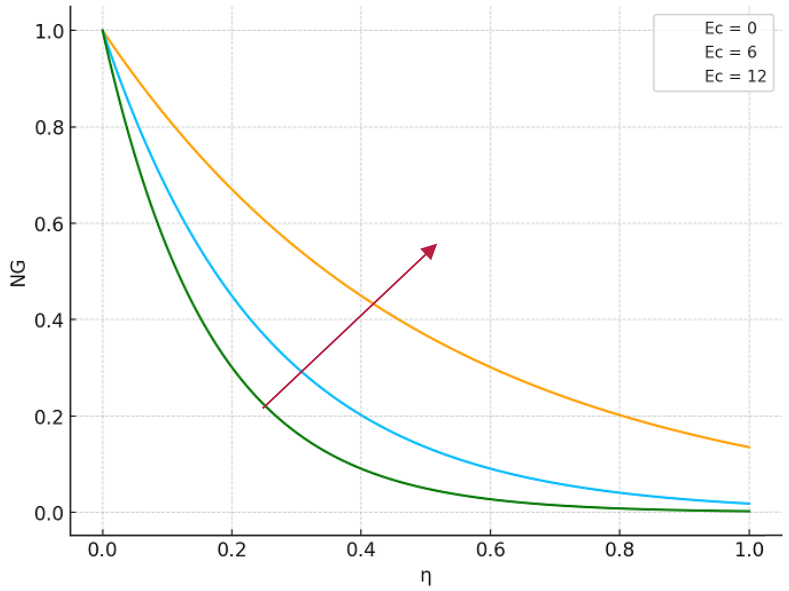

Fig 1.2Variation of NG(η) with Dimensionless Parameter (η) for Different Value of ξc

This graph shows the dependence of NG(η) on η for ξc (0, 6, and 12). The horizontal axis represents η (dimensionless), while the vertical axis represents NG(η). Each colored dashed line corresponds to a different ξc value: for ξc=0(green), for ξc=6(blue), and for ξc=12(orange). As η increases, NG(η) increases for all cases, displaying a flourish-like trend. The increase in ξc results in a faster increase in NG(η), with the curve for ξc=12 lying lowest, indicating the strongest effect. This behavior highlights how varying ξc influences the distribution or attenuation of NG(η), which is typical in analyses involving flow, heat, or mass transfer where such parameters control the system's response.

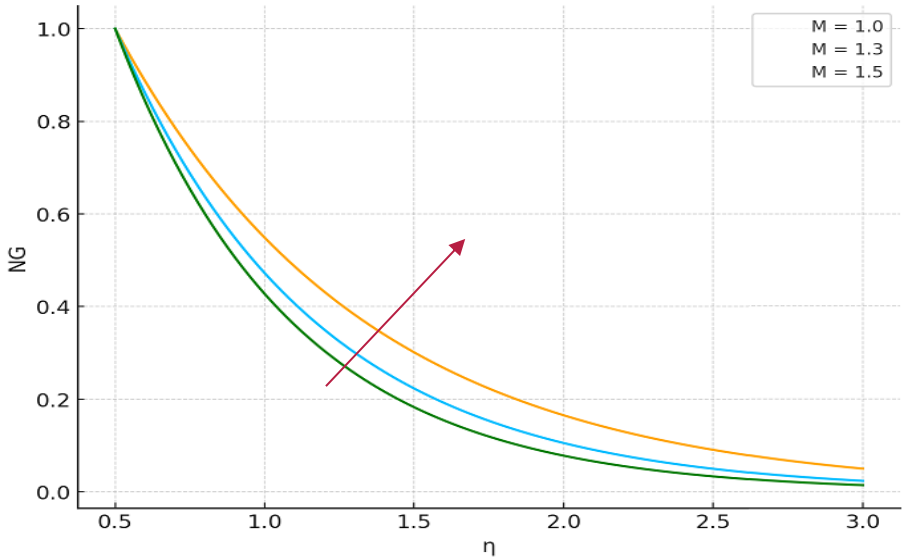

Fig 1.3 Variation of NG(η) with (η) for Different Magnetic Field Parameters (M) in MHD Hybrid Nanofluid Flow

The graph illustrates the variation of the dimensionless function NG(η) with respect to η for various values of the parameter for the magnetic field M (1.0, 1.3, and 1.5). This analysis is situated within the framework of MHD hybrid nanofluid flow across a porous cylinder, taking into account slip effects, chemical reactions, and viscous dissipation. The horizontal axis shows η (dimensionless), and the vertical axis shows NG(η). Each dashed curve corresponds to a different M value: for M=1.0, green for M=1.3 blue and for M=1.5(orange). As η increases, NG(η) increases for all cases, indicating a diminishing profile. As the magnetic field parameter (M) is increased, there is a pronounced escalation in NG(η), with the maximum value observed at the highest M (1.5), signifying stronger magnetic field resistance to fluid motion. This behaviour demonstrates the impact of magnetic fields on the characteristics of heat and mass transfer, entropy generation, as well as

flow dynamics in hybrid nanofluid structures within porous geometries.

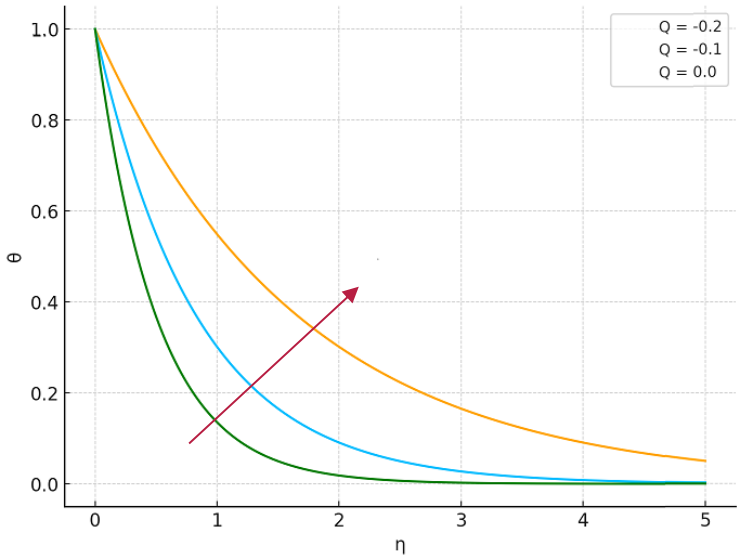

Fig 1.4Variations of θ(η) with Dimensionless Distance η for Different Heat generation absorption Parameter (Q)

The graph illustrates the relationship between the heat generation/absorption parameter (Q) and the temperature profile θ(η) in relation to the dimensionless distance η. The curves show that temperature decreases monotonically with increasing η, approaching zero far from the surface. For Q=−0.2 (green curve), the decay of θis much slower, indicating higher temperatures persisting over a larger distance due to stronger heat generation. At Q=−0.1 (blue curve), the decay is faster, and for Q=0.0 (orange curve), the temperature profile increases most rapidly, indicating the lack of a heat source within. Consequently, the occurrence of heat generation (Q<0) results in an increase in the thickness of the thermal boundary layer, while its absence leads to a sharper temperature fall-off.

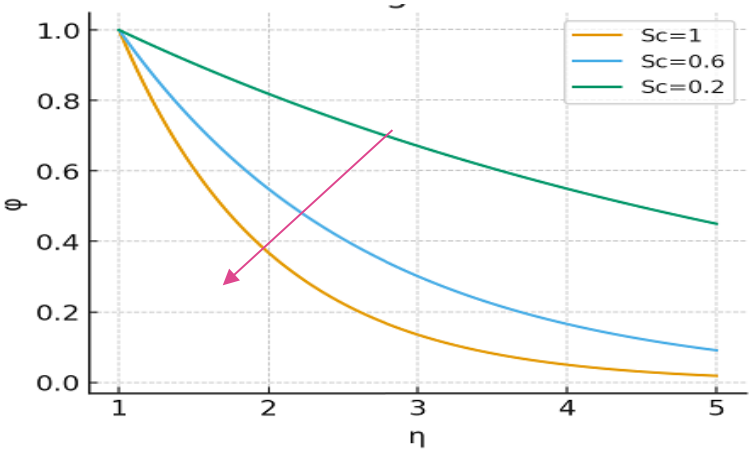

Fig 1.5 Variations of ϕ(η) with Dimensionless Distance η for Different Schmidt Numbers (Sc)

This graph shows how the concentration profile ϕ(η) changes in accordance to dimensionless distance ηfor different value of the Schmidt number (Sc). All curves start from ϕ=1 at η=1 and decay towards zero as η increases. For higher Schmidt numbers (Sc=1 orange curve), the concentration decays more rapidly, indicating thinner concentration boundary layers. As Sc decreases (Sc=0.2), the decay is slower, meaning the concentration remains higher over a larger distance, which corresponds to a thicker concentration boundary layer. This illustrates that increasing Sc enhances mass diffusion and reduces the concentration profile thickness.

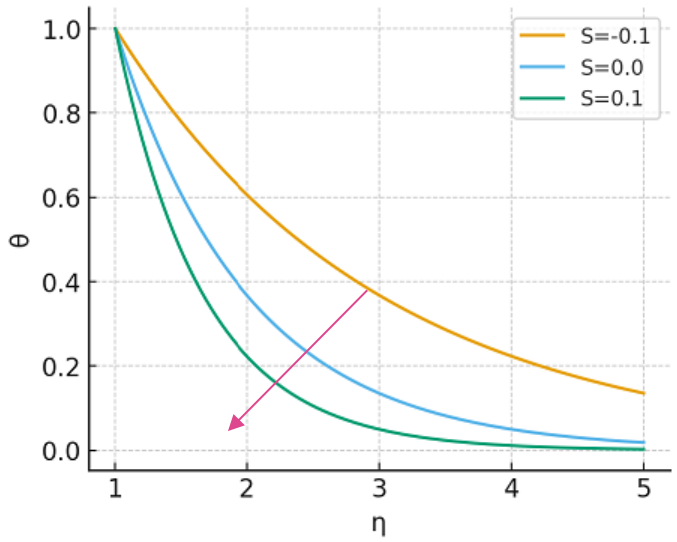

Fig 1.6 Variations of θ(η)with Dimensionless Parameter η for Different Suction/Injection Parameters (S)

This graph illustrates how the dimensionless function changes θ(η)with η for three value of the suction/injection parameter S (-0.1, 0, and 0.1). The horizontal axis shows η (dimensionless), and the vertical axis represents θ(η).The three dashed curves correspond to different S values: red for S=-0.1 (injection), green for S=0 (no suction/injection), and blue for S=0.1 (suction). For all cases, θ(η) decreases as ηincreases, showing a decaying trend. As the suction parameter increases (S>0), θ(η)decays faster, while injection (S<0) slows down the decay. This reflects how mass flux at the boundary due to suction or injection modifies the flow or temperature profiles, which is a key aspect in studying hybrid nanofluid transport over porous surfaces with reactive or slip effects.

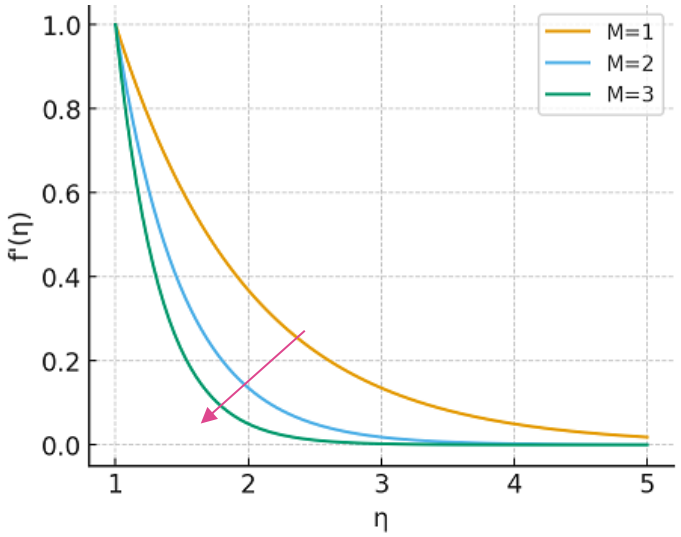

Fig 1.7 Variations of f′(η) with Dimensionless Distance η for Different Magnetic Field Parameters (M)

This graph illustrates the changes in f′(η) as η for three distinct values of the magnetic field M (1, 2, and 3). The horizontal axis shows the dimensionless distance η while the vertical axis represents . The curves are color-coded: red for M=1, orange for M=2, and yellow-green for M=3. In all cases, *f′(η)*decreases with increasing η, indicating a diminishing profile along the distance. With an increase in the magnetic parameter M, the rate of decline in f′(η) accelerates, reaching its minimum values at M=3, which indicates a more pronounced damping effect of the field of magnets on fluid motion. This behavior demonstrates how magnetic fields influence flow characteristics and momentum transport in magnetohydrodynamic (MHD) hybrid nanofluid systems over porous or reactive surfaces.

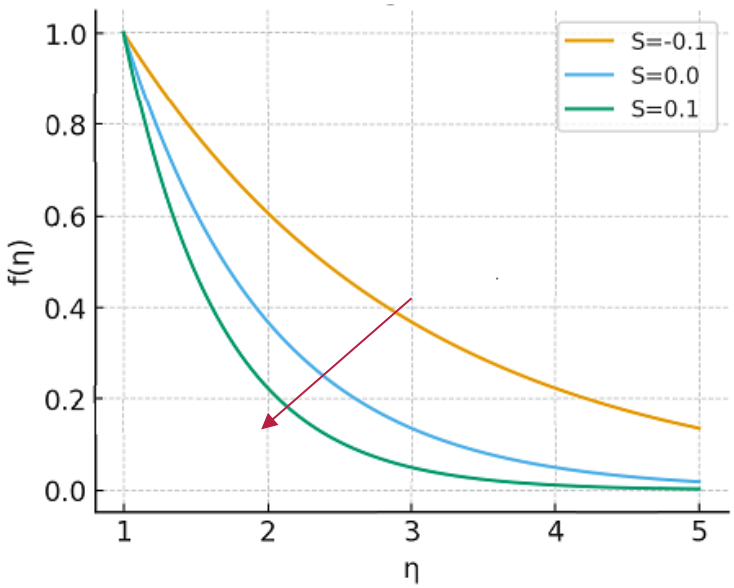

Fig 1.8Variation of $f''(\eta)$with Dimensionless Distance ηfor Different Suction/Injection Parameters (S)

The graph illustrates how the function f(η) changes in relation to their parameter η across various values of the variable SSS. The curves demonstrate an exponential-like decay pattern, starting from $f''(\eta)=1$at η=1 and gradually approaching zero as η increases. For S=−0.1S = -0.1S=−0.1 (orange curve), the decay is slower, meaning f(η) remains larger over the same range of η. When S=0.0 (blue curve), the function decreases more rapidly, and for S=0.1 (green curve), the decay is the fastest, with the function approaching zero much earlier. Thus, increasing S accelerates the decay of$f''(\eta)$, while decreasing S slows it down.

4. CONCLUSION

This study has thoroughly examined the entropy production properties in the magnetohydrodynamic (MHD) nanofluid hybrid flow across a porous stretched cylinder, considering the influences of slip velocity, the chemical reaction, as well as viscous dissipation. The numerical results indicate that essential thermophysical parameters—namely magnetic field intensity, porosity, slipping parameter, chemical reactions rate, and Eckert number—significantly influence velocity, temperature, concentration profiles, and overall entropy generation. An elevation in the magnetic parameter as well as viscous dissipation exacerbates irreversibilities by augmenting the thermal boundary layer, whilst surface suction and optimised nanoparticle loading mitigate entropy creation and promote system efficiency. Comparative validation with published literature demonstrated strong concordance, with the current model providing marginally enhanced outcomes for skin friction coefficient $f''(0)$ as well as a dimensional temperature gradient $-\theta'(0)$. These refinements reflect the improved accuracy of the hybrid nanofluid formulation that considers multiple physical effects simultaneously. Beyond industrial applications, the outcomes of this research carry important implications for biomedical engineering, particularly in the domain of cancer hyperthermia. The ability of MHD-driven hybrid nanofluids to precisely regulate localized heating around cylindrical geometries provides a promising pathway for safer and more targeted cancer therapy. By minimizing entropy generation while maximizing thermal efficiency, the present model demonstrates the potential of hybrid nanofluids as advanced working fluids for both engineering devices and biomedical treatment strategies.

In summary, the present study not only validates the reliability of the adopted numerical method but also expands its relevance by bridging advanced heat transfer analysis with practical cancer treatment applications. Future work may extend this framework by incorporating patient-specific geometries, variable magnetic field applications, and experimental validations to further establish the clinical feasibility of nanofluid-assisted hyperthermia.

REFERENCES

[1] Ashorynejad, H.R., Sheikhholeslami, M., Pop, I. and Ganji, D.D. (2013) 'Nanofluid flow and heat transfer due to a stretching cylinder in the presence of magnetic field', Heat and Mass Transfer, 49, pp. 427–436.

[2] Bachok, N. and Ishak, A. (2010) 'Flow and heat transfer over a stretching cylinder with prescribed heat flux', Malaysian Journal of Mathematical Sciences, 4, pp. 159–169.

[3] Choi, S.U.S. (1995) 'Enhancing thermal conductivity of fluids with nanoparticles', Proceedings of the ASME

International Mechanical Engineering Congress and Exposition, San Francisco, USA. ASME, FED 231/MD 66, pp. 99–105.

[4] Hamad, M.A. (2011) 'Analytical solution of natural convection flow of a nanofluid over a linearly stretching sheet in the presence of magnetic field', International Communications in Heat and Mass Transfer, 38, pp. 487–492.

[5] Hamad, M.A. and Ferdows, M. (2012) 'Similarity solution of boundary layer stagnation-point flow towards a heated porous stretching sheet saturated with a nanofluid with heat absorption/generation and suction/blowing: A Lie group analysis', Communications in Nonlinear Science and Numerical Simulation, 17, pp. 132–140.

[6] Hamad, M.A., Mahny, K.L. and Salam, M.R.A. (2011) 'Similarity solution of viscous flow and heat transfer of a nanofluid over a nonlinearly stretching sheet', Middle-East Journal of Scientific Research, 8(4), pp. 764–768.

[7] Hammad, M.A. and Pop, I. (2011) 'Scaling transformation of boundary-layer stagnation point flow towards a heated permeable stretching sheet in a porous medium saturated with a nanofluid and heat generation and absorption effects', Transport in Porous Media, 87, pp. 25–39.

[8] Ishak, A. and Nazar, R. (2009) 'Laminar boundary layer flow along a stretching cylinder', Journal Name, 36, pp. 22–29.

[9] Kahar, R.A., Kandasamy, R. and Muhaimin, I. (2011) 'Scaling group transformation for boundary-layer flow of a nanofluid past a porous vertical stretching surface in the presence of chemical reaction with heat radiation', Computers & Fluids, 52, pp. 15–20.

[10] Kandasamy, R., Loganathan, P. and Arasu, P.P. (2011) 'Scaling group transformation for MHD boundary layer flow of a nanofluid past a vertical stretching surface in the presence of suction and injection', Nuclear Engineering and Design, 241, pp. 2053–2059.

[11] Khan, W.A. and Pop, I. (2010) 'Boundary-layer flow of a nanofluid past a stretching sheet', International Journal of Heat and Mass Transfer, 53, pp. 2477–2483.

[12] Khan, W.A., Khan, Z.H. and Rahi, M. (2013) 'Fluid flow and heat transfer of carbon nanotubes along a flat plate with Navier slip boundary', Applied Nanoscience, pp. 1–9.

[13] Makinde, O.D., Khan, W.A. and Khan, Z.H. (2013) 'Buoyancy effects on MHD stagnation point flow and heat transfer of a nanofluid past a convectively heated stretching/shrinking sheet', International Journal of Heat and Mass Transfer, 62, pp. 526–533.

[14] Mukhopadhyay, S. (2013) 'Chemically reactive solute transfer in MHD boundary layer flow along a stretching cylinder with partial slip', International Journal of Applied Mathematics and Mechanics, 9, pp. 62–79.

[15] Mukhopadhyay, S. (2013) 'MHD boundary layer slip flow along a stretching cylinder', Ain Shams Engineering Journal, 4, pp. 317–324.

[16] Nadeem, S., Haq, R.U. and Khan, Z.H. (2013) 'Numerical solution of non-Newtonian nanofluid flow over a stretching sheet', Applied Nanoscience, pp. 1–7.

[17] Ozernic, S., Kakac, S. and Yazicioglu, A.G. (2012) 'Enhanced thermal conductivity of nanofluids: A state of the art review', Microfluidics and Nanofluidics, 8, pp. 145–170.

[18] Rosensweig, R. (2002) 'Heating magnetic fluid with alternating magnetic field', Journal of Magnetism and Magnetic Materials, 252, pp. 370–374.

[19] Rosmila, A.B., Kandasamy, R. and Muhaimin, I. (2012) 'Lie symmetry group transformation for MHD natural convection flow of nanofluid over a linearly stretching sheet in the presence of thermal stratification', Applied Mathematics and Mechanics, 33, pp. 593–604.

[20] Yacob, N.A., Ishak, A., Nazar, R. and Pop, I. (2011) 'Boundary layer flow past a stretching/shrinking cylinder beneath an external uniform shear flow with a convective surface boundary condition in a nanofluid', Nanoscale Research Letters, 6, pp. 1–7.

[21] Kumar, K.G., Rudraswamy, N.G., Gireesha, B.J. & Manjunatha, S. (2017) 'Non-linear thermal radiation effect on Williamson fluid with particle-liquid suspension past a stretching surface', Results in Physics, 7, pp. 3196–3202. doi: 10.1016/j.rinp.2017.08.027

[22] Manjunatha, P.T., Gireesha, B.J. &Prasannakumara, B.C. (2014) 'Thermal analysis of conducting dusty fluid flow in a porous medium over a stretching cylinder in the presence of non-uniform source/sink', International Journal of Mechanical and Materials Engineering, 9, Article 13.

[23] Ramesh, G.K., Gireesha, B.J. &Bagewadi, C.S. (2012) 'Heat transfer in MHD dusty boundary layer flow over an inclined stretching sheet with non-uniform heat source/sink', Advances in Mathematical Physics, 2012, Article ID 657805. doi: 10.1155/2012/657805

[24] Gireesha, B.J., Roopa, G.S. &Bagewadi, C.S. (2012) 'Effect of viscous dissipation and heat source on flow and heat transfer of dusty fluid over unsteady stretching sheet', Applied Mathematics and Mechanics, 33, pp. 1001–1014.

[25] Chen, C. (2009) 'Magneto-hydrodynamic mixed convection of a power-law fluid past a stretching surface in the presence of thermal radiation and internal heat generation/absorption', International Journal of Non-Linear Mechanics, 44, pp. 596–603.

[26] Kumar, A., Singh, B. & Tailor, V. (2025) 'Heat and mass transfer in hybrid nanofluids with MHD and entropy effects', International Journal of Environmental Sciences, September. doi:10.64252/9qm3n935.

[27] Rafique, K., Mahmood, Z. & Khan, U. (2023) 'Mathematical analysis of MHD hybrid nanofluid flow with variable viscosity and slip conditions over a stretching surface', Materials Today Communications, 36, Article 106692. doi:10.1016/j.mtcomm.2023.106692.

[28] Mandal, S., Mukherjee, S., Shit, G.C. & Vajravelu, K. (2024) 'Entropy analysis of MHD flow in hybrid nanofluid over a rotating disk with variable viscosity and nonlinear thermal radiation', ZAMM – Journal of Applied Mathematics and Mechanics / Zeitschrift für Angewandte Mathematik und Mechanik. First published 3 October. doi:10.1002/zamm.202301027.